Received: 5 January 2021 | Accepted: 7 October 2021

DOI: 10.1002/vzj2.20173

Vadose Zone Journal

ORIGINAL RESEARCH ARTICLE

Experiment for validation of numerical models of coupled heat and mass transfer around energy cables

Christoph Verschaffel-Drefke[1,2] | **Constantin Balzer**[2,3] | **Markus Schedel**[1,2] | **Volker Hinrichsen**[2,3] | **Ingo Sass**[1,2]

[1] Dep. of Materials and Earth Sciences, Geothermal Science and Technology, Technical Univ. of Darmstadt, Schnittspahnstr. 9, Darmstadt 64287, Germany

[2] Darmstadt Graduate School of Excellence Energy Science and Engineering, Technical Univ. of Darmstadt, Otto-Berndt-Str. 3, Darmstadt 64287, Germany

[3] Dep. of Electrical Engineering and Information Technology, High-Voltage Laboratories, Technical Univ. of Darmstadt, Fraunhoferstr. 4, Darmstadt 64283, Germany

Correspondence
Christoph Verschaffel-Drefke, Dep. of Materials and Earth Sciences, Geothermal Science and Technology, Technical Univ. of Darmstadt, Schnittspahnstr. 9, 64287 Darmstadt, Germany.
Email: drefke@geo.tu-darmstadt.de

Assigned to Associate Editor Eva Kroener.

Funding information
E.ON Innovation Center Distribution and Bayernwerk AG; Darmstadt Graduate School of Excellence Energy Science and Engineering

Abstract

The increasing decentralization of electrical energy production as well as an increasing number of fluctuating regenerative energy sources require significant investments in grid expansion. Among other assessments, an exact prediction of the thermal behavior of the cable environment is necessary to be able to design cable routes both technically and economically sufficient. To investigate the coupled thermal and hydraulic processes around a cable-like heat source with high temporal and spatial resolution under controlled boundary conditions, a cylindrical laboratory test was designed and experiments with two soils conducted. The data collected can be used to validate models of coupled heat and mass transfer around power cables. Within this study, the experimental data was compared with a modified model approach that is based on experimentally determined input data for the thermal and hydraulic properties of the examined soils. Although overall good agreement in the temperature field around the central heat source was observed, differences in the spatial distribution of the dry-out zone near the heat source led to some shift between the measured and simulated temperatures.

1 | INTRODUCTION

The importance of the thermal properties of the bedding material with respect to ampacity calculations of buried energy cables is undisputed. However, in contrast with the usually well-known thermo-physical properties of the cable construction materials, the integration of adequate properties for the surrounding cable bedding and soil still represents a major difficulty. Besides natural heterogeneities such as different soil types or bulk densities, this is particularly related to the influence of variable water contents at common installations depths for buried electric cables of about 0.5–2.0 m.

Abbreviations: PVC, polyvinyl chloride; TCDC, thermal conductivity dry-out curve; UHCC, unsaturated hydraulic conductivity characteristic; WRC, water retention characteristic.

In unsaturated porous media such as soils, the total heat transfer can be described as a sum of conductive heat transfer, convective heat transfer due to mass flow of the mobile phases (i.e., the soil air and water within pore space) and latent heat transport due to water vapor migration (Philip & de Vries, 1957). For cable installation located in the vadose zone, nearly all important thermal and hydraulic properties of the cable surrounding strongly depend on the water content. For example, a change in the water content of a bedding might result in changes of almost one order of magnitude of its thermal conductivity. For buried electric cables, another effect as a result of the coupled heat and mass transfer processes within the bedding is also important for the technical design of the system: the heat that is dissipated by the power cable leads to moisture migration away from the cable, which entails further reduction of the water content in the vicinity of cables (Brakelmann, 1984). This self-reinforcing process (often referred to as "thermal runaway") might lead to an excess of the conductor temperature above the maximum permissible value, hence putting the cable at risk of accelerated aging or—at worst—an insulation breakdown. Conventional methods for calculating the cable ampacity only consider the conductive heat transport and try to account for these effects with the so-called two-zone model of partial soil drying. In this approach, the cable bedding initially has a homogeneous thermal conductivity until a critical temperature is exceeded. At this temperature, a sudden change to a dry thermal conductivity is assumed (Brakelmann, 1984).

However, for some applications such as complex bedding geometries, these assumptions might be oversimplified and it is not surprising that considerable effort was made to theoretically describe the phenomena of coupled heat and mass transfer mechanisms within cable beddings and soil. The fundamental approach of Philip and de Vries (1957) represents the basis of most contributions, reducing the complex microscopic transfer phenomena within soils in general to four macroscopically described transport phenomena. Most recently, this approach was used to study the effect of drying-out mechanisms in the framework of a realistic operation of energy cables (Anders & Radhakrishna, 1988; Freitas et al., 1996; Groeneveld et al., 1984; Hruška et al., 2018; Kroener et al., 2014, 2017; Radhakrishna et al., 1984; Snijders et al., 1981). Most of the studies have a strong theoretical or numerical approach and lack of experimental data for proper validation purposes. Especially for the application of buried electric cables, suitable test setups with configurations that reproduce the physical dimensions around buried cables at defined boundary conditions, combined with a high-resolution data acquisition, is missing. Furthermore, in publications that compare experimental data with a model approach, sensitive input variables of the used soils were only estimated and not experimentally determined (Groeneveld et al., 1984; Kroener et al., 2014; Saito et al., 2006; Snijders et al., 1981). A majority of the recent work is also limited to investigations of sandy soils or loamy sands (Anders & Radhakrishna, 1988; Freitas et al., 1996; Groeneveld et al., 1984; Saito et al., 2006; Snijders et al., 1981). Cohesive soils, on the other hand, differ fundamentally in their hydraulic properties and consequently in their drying-out behavior.

Core Ideas

- A validation experiment for simulations of heat dissipation of power cables was conducted.
- Drying-out processes in the vicinity of buried power cables were investigated.
- The thermal and hydraulic properties of bedding materials were experimentally determined.

For this study, a large-scale tank experiment was developed to deliver experimental data of the two-dimensional propagation of drying processes around a cable-like heat source. To enable the validation of models of coupled heat and mass transfer around power cables with the experimental setup, the temperature as well as the matric potential was measured in high spatial resolution within the experiment. Furthermore, in order to validate the applicability of models for different soil types, two entirely different natural soils were investigated: a sandy soil with a uniform grain size distribution, referred to here as "sandy soil"; and a very nonuniform and considerably fine-grained soil, referred to here as "clayey soil." All relevant input data necessary for models of coupled heat and mass transfer were experimentally determined for both soils. Within the study the experimental data were used to compare the experiment with a finite element simulation of a modified model based on the approach of Philip and de Vries (1957). For this model, experimentally determined input data were used, and possible temperature dependencies were taken into account.

2 | MATERIAL AND METHODS

2.1 | Experimental setup

The large-scale tank experiment (Figure 1) consisted of a sealed-off cylindrical steel tank serving as an outer boundary condition and an inner pipe as a central heat source. During the experiment, the space between the outer steel tank and the central heat source was filled with compacted soil. The outer steel tank was made out of a large diameter steel

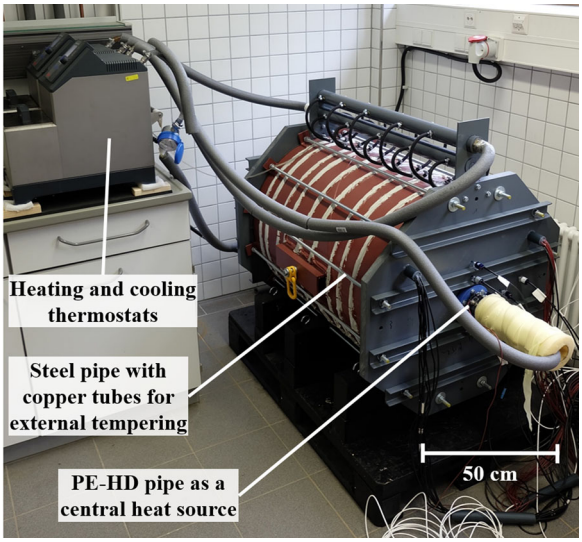

FIGURE 1 Tank experiment to study heat and mass transfer in the vicinity of a simulated underground cable (additional external thermal insulation not mounted for better illustration purposes). PE-HD, high-density polyethylene

pipe and had an inner diameter of 635 mm at a length of 872 mm. The outer diameter of the inner pipe was 64 mm. To obtain a thermal contact resistance of the simulated cable to the bedding comparable to real buried cables, the inner pipe consisted of high-density polyethylene like typical cable surfaces.

The complete experimental setup was developed to ensure two-dimensional heat and mass transport in the central area of the apparatus. Thus, for the experiments, the sides of the tank were sealed with low thermal conductive polyvinyl chloride (PVC) plates. The sensors were installed with each bedding material in an upright position of the tubes in accordance with geotechnical requirements. For this purpose, the tank experiment was firstly sealed by a PVC plate on its bottom side. After completely filling the space between the tubes, the assembly was sealed on top by an identical PVC plate, and the entire test setup was rotated into a horizontal position. An equilibration of the pore air pressure within the system with the atmosphere was secured by several tiny tubes (0.8 mm in diameter) installed through both PVC plates.

The temperatures of steel tank and central heat pipe were controlled by a circulating heat carrier fluid (water with glycol) via thermostats. The heat carrier fluid passed directly through the inner pipe. The temperature of the outer steel tube was controlled by several rounds of copper tubes attached to the outside of the steel tube (Figure 1). To simulate the heating of a power cable the central pipe was heated controlling the temperature of the heat carrier fluid. During the experiments, mainly rectangular pulses of different time durations (2–240 h) and temperatures in the range from 33 to 83 ˚C were performed. The steel tank was tempered at the outside with a constant temperature of 23 ˚C. The experiments with a total of three different beddings installed lasted in total for a period of 18 mo.

In order to verify both transfer mechanisms, the distributions of temperature as well as the water content had to be recorded during the heating cycles of the central heat source. The temperatures were measured directly by 15 Pt 100 resistance thermometers {accuracy $\pm$ [0.03 K + 0.0005 (T − 273.15 K)]}. Since water content measurements with frequency domain reflectometry (FDR) or time-domain reflectometry (TDR) measuring technology are highly dependent on the electrical conductivity and thus on the temperature, the hydraulic changes were determined by the much more robust measurement of the matric potential by means of seven T5 laboratory tensiometers from the manufacturer METER Group AG (accuracy $\pm$ 0.05 m). The sensors were placed in the plane perpendicular to the direction of the cable as illustrated in Figure 2. The spatial arrangement of each sensor was measured both before and after the test. The deviations of these measurements in all spatial directions were below 3 mm.

2.2 | Investigated soils and determined input parameters

To enable for a more general validation of models, the investigations were carried out using two completely different types of soil, a sandy and a clayey soil. The soils were thoroughly investigated in the laboratory (Table 1). In preceding field investigations of these soils, it was found that for the sandy soil, an initial saturation of about 32% matches real site conditions in placement depth of cables after a humid season (Drefke et al., 2015). The saturation of 14% for the second investigation of the sandy soil corresponds to the mean water content that was measured after a summer period. The saturation of 82% for the clayey soil corresponds to the annual mean water content in laying depth of the cables. Prior to the installation of the beddings in the tank experiment, the soils were homogenized using a soil mixer and their water content was adjusted (Table 1).

For simulations of the water transport in unsaturated soils, the water retention characteristic (WRC) and the unsaturated hydraulic conductivity characteristic (UHCC) are required. The dependence of the thermal conductivity on the water content, referred to as the thermal conductivity dry-out curve (TCDC), is required in order to calculate the heat transfer. All three characteristics can be determined for a sample in one experiment with the evaporation test according to Drefke et al. (2017), which represents further development of the evaporation test according to Schindler et al. (2010).

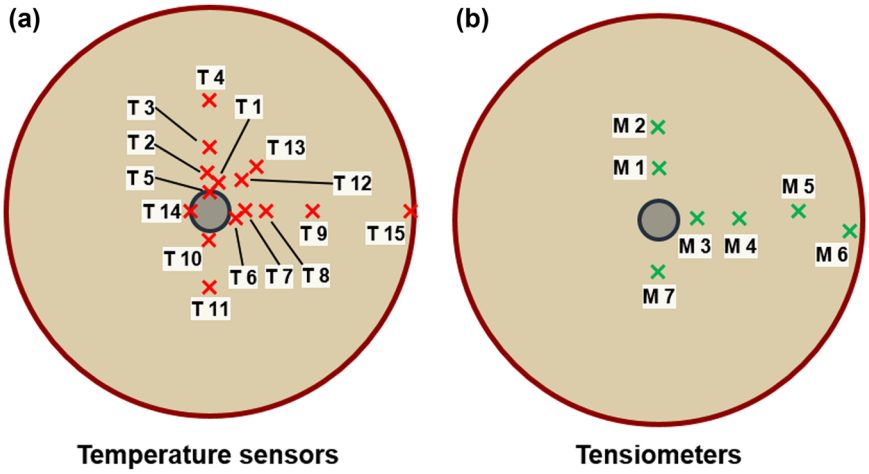

FIGURE 2 Spatial allocation of the sensors, each in a cross section through the tank experiment. Pt 100 temperature sensors in a cross section (a) in the center of the tank, tensiometers in a cross-section 20 cm from the top plate (b)

TABLE 1 Geotechnical, thermal, and hydraulic parameters of the investigated materials

		Test series		
		Sandy soil		Clayey soil
Parameter	**Units**	**I**	**II**	**III**
Grain size distribution				
d_{10}	mm	0.089	0.089	<0.001
d_{30}	mm	0.142	0.142	0.008
d_{50}	mm	0.199	0.199	0.043
d_{60}	mm	0.230	0.230	0.078
Packing				
Dry soil density, ρ_d	g cm^{-3}	1.62	1.61	1.76
Porosity, φ	m^3 m^{-3}	0.39	0.39	0.36
Grain density, ρ_g	g cm^{-3}	2.64	2.64	2.75
Water content				
Gravimetric, w	%	7.76	3.39	16.71
Volumetric, θ	%	12.50	5.45	29.40
Saturation, S	%	32	14	82
Measured thermal conductivity, λ (20 ˚C)				
At water content	W m^{-1} K^{-1}	1.58	1.29	1.56
Dry	W m^{-1} K^{-1}	0.50	0.49	0.84
Saturated	W m^{-1} K^{-1}	2.26	2.22	1.58
Saturated hydraulic conductivity, k_{sat} (measured after ISO 17892-11)	m s^{-1}	2.06×10^{-5}	2.34×10^{-5}	5.03×10^{-6}

2.2.1 | Water retention characteristic

Due to hysteresis, the actual WRC starting from a certain initial point ranges between the main wetting and main drainage curve (Figure 3). To map any course of a WRC, the hysteresis model after Scott et al. (1983) requires at least information about the course of the main wetting and main drainage curve. With the conducted evaporation test, data points of the WRC could be determined continuously, but only during drying of the specimen. Therefore, the main drainage of the WRC was measured, whereas the course of the main irrigation had to be determined in a different way. A selective measurement of the matric potential with stepwise irrigation of previously dried samples was conducted. For this purpose, a corresponding amount of water was added to the initially dry samples from their bottom side without additional pressure. After some days of equilibration, the data points of the main wetting curve were generated by measuring the matric potential of these samples. The measurement results for the examined samples of the two soils are displayed in Figure 3.

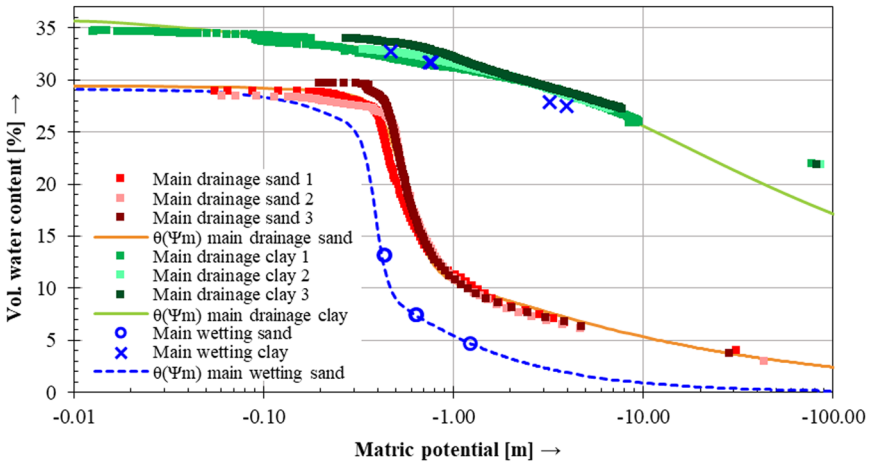

FIGURE 3 Measured water retention characteristic data points and fitted hydraulic functions $\theta(\Psi_m)$ for the main drainage and main wetting curve of the sandy soil and for the main drainage of the clayey soil

In order to transform the data points (taken by repeated measurements on three specimens per soil) into the desired steady hydraulic function, the parameterized bimodal van Genuchten model (Durner, 1994) was used.

$$S_{\text{eff}}\left(\Psi_m\right) = \sum_{j=1}^{2} \omega_j \left(1 + \left(\alpha_j \left|\Psi_m\right|\right)^{n_j}\right)^{-m_j} = \sum_{i=1}^{2} \omega_i S_i \tag{1}$$

with $m = 1 - n^{-1}$ and $\omega_1 + \omega_2 = 1$, where ω, α (m^{-1}), and n are fitting parameters, and Ψ_m (m) is the matric potential.

The effective saturation S_{eff} is related to the absolute water content θ ($m^3\ m^{-3}$) as follows:

$$\theta\left(\Psi_m\right) = S_{\text{eff}}\left(\Psi_m\right)\left(\theta_s - \theta_r\right) + \theta_r \tag{2}$$

where θ_s ($m^3\ m^{-3}$) is the saturation- and θ_r ($m^3\ m^{-3}$) the residual-water content.

The experimental data presented in Figure 3 show high reproducibility of the conducted measurements and exemplify that hysteresis is especially pronounced in coarse-grained soils (Hillel, 1980). A comparison of main drainage and wetting measurements of both soils show that the sandy soil exhibits a pronounced hysteresis, whereas it is almost nonexistent in the investigated clayey soil. Due to the negligible hysteresis of the clayey soil, its consideration was waived, and the hydraulic function only fitted to the data of the main drainage. Since the WRC function according to Durner (1994) is coupled with the hydraulic conductivity function (see paragraph below), a fitting of the two functions was performed simultaneously. The fitting was done by using special evaluation software (Hyprop Data Evaluation Software, Meter Group AG). The parameters determined are summarized in Table 2. The algorithm minimizes the sum of squared deviations between data points and the fitted functions (Pertassek et al., 2011; Peters et al., 2015). This method minimizes errors in areas where, for example, there are WRC data but no hydraulic conductivity data and vice versa. In order to obtain the desired function that is implemented in the simulation, the fitting of the model of Durner (1994) to all data points was adapted to all data points of each drainage (and irrigation) cycle of a material.

2.2.2 | Unsaturated hydraulic conductivity characteristic

Figure 4 displays the measured UHCC from the evaporation experiment with the fitted hydraulic functions. Although the natural sample material was elaborately homogenized and the samples were taken carefully, there are small differences between the measurements of the different specimen. Nevertheless, it should be taken into account that an estimation of the hydraulic conductivity (e.g., derived from particle size distribution) can lead to values deviating by several orders of magnitude from the real value. For these reasons, a measurement is always preferable to an estimation.

The combination of the used WRC with the UHCC in accordance with Mualem (1976) yields the following expression of the relative hydraulic conductivity function (Priesack & Durner, 2006):

$$k_r\left(S_{\text{eff}}\right) = \left(\sum_{i=1}^{2} \omega_i S_{\text{eff}\,i}\right)^{\tau} \left\{\frac{\sum_{i=1}^{2} \omega_i \alpha_i \left[1 - \left(1 - S_{\text{eff}}^{\,1/m_i}\right)^{m_i}\right]}{\sum_{i=1}^{2} \omega_i \alpha_i}\right\}^2 \tag{3}$$

The unsaturated hydraulic conductivity k_u (m^{-1}) results from the multiplication of the relative conductivity k_r (–) with the saturated hydraulic conductivity k_{sat} (m^{-1}):

$$k_u\left(S_{\text{eff}}\right) = k_{\text{sat}} k_r\left(S_{\text{eff}}\right) \tag{4}$$

TABLE 2 Fitting parameters of the used hydraulic models for both soils

Parameter	Units	Sandy soil		Clayey soil
		Main drainage	Main irrigation	Main drainage
van Genuchten parameters				
α_1	m^{-1}	0.29469	3.10194	40.4943
n_1	–	1.35266	1.83110	1.09366
θ_r	$m^3\ m^{-3}$	0	0	0
θ_s	$m^3\ m^{-3}$	0.291071	0.291071	0.360000
α_2	m^{-1}	1.83399	2.600154	0.214282
n_2	–	6.0389	14.00185	1.23414
w_2	–	0.667911	0.510000	0.652849
Mualem parameters				
k_s	$m\ s^{-1}$	3.66×10^{-6}	3.66×10^{-6}	4.79×10^{-7}
τ	–	1.52	3.20	−6.00

Note. α_1, α_2, n_1, n_2, θ_r, θ_s, and w_2 are fitting parameters for the hydraulic function of Durner (1994) for retention. k_s and τ are fitting parameters for the associated hydraulic conductivity function after Mualem (1976).

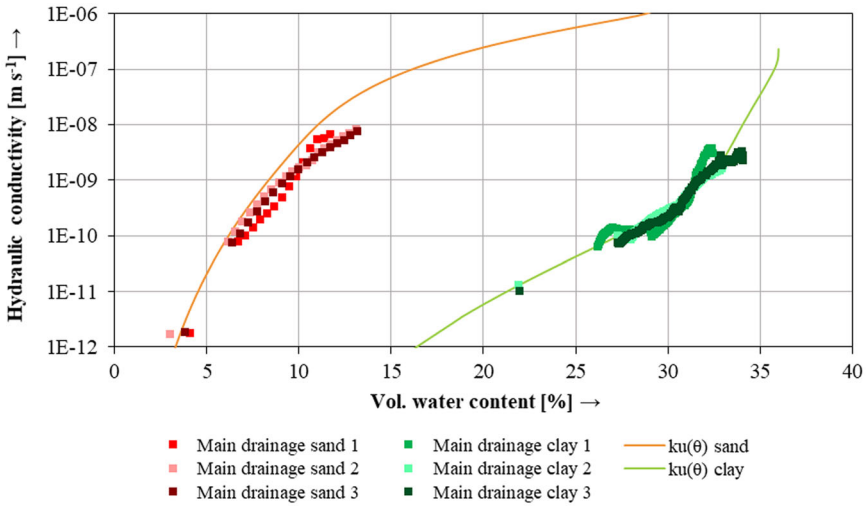

FIGURE 4 Measured unsaturated hydraulic conductivity characteristic data points and fitted hydraulic functions $k_u(\theta)$ of the sandy and clayey soil

2.2.3 | Thermal conductivity dry-out curve

The TCDC measurements presented in Figure 5 were recorded during the evaporation test using a KD2 Pro thermal needle probe (Decagon Devices). Regardless of the measurement method the overall effective or apparent thermal conductivity λ (W m^{-1} K^{-1}) is measured. This value, in case of a partially saturated soil, is always influenced by the occurrence of latent heat transfer. The proportion of actual conduction on the overall heat transfer is represented by the (conductive) thermal conductivity λ', which can be determined from the measured apparent thermal conductivity λ at 20 °C using Equation 31. To highlight the influence of elevated temperatures on the apparent thermal conductivity, calculated values of λ at 60 °C using Equation 31 are displayed in Figure 5 as well. The course of the TCDC shows the typical nonlinear relationship resulting mainly from the rapid change of water menisci between the soil solid particles predominantly at critical water contents in the dry area. As expected, this effect is more pronounced for the sandy soil compared with the clayey soil. The nonlinear pore size distribution and the associated distribution of water menisci during drainage might be the reason for the notable step in the TCDC of the sand at a θ around 22%. From Figure 5, it also becomes clear that the difference between the apparent λ and the (conductive) thermal conductivity λ' can be neglected at 20 °C. In contrast, at higher temperatures, mass transfer processes have an increasing influence on the apparent thermal conductivity. Since its magnitude is strongly associated with the feasible latent heat transfer, the apparent thermal conductivity decreases at low as well as high saturations and reaches its peak in between.

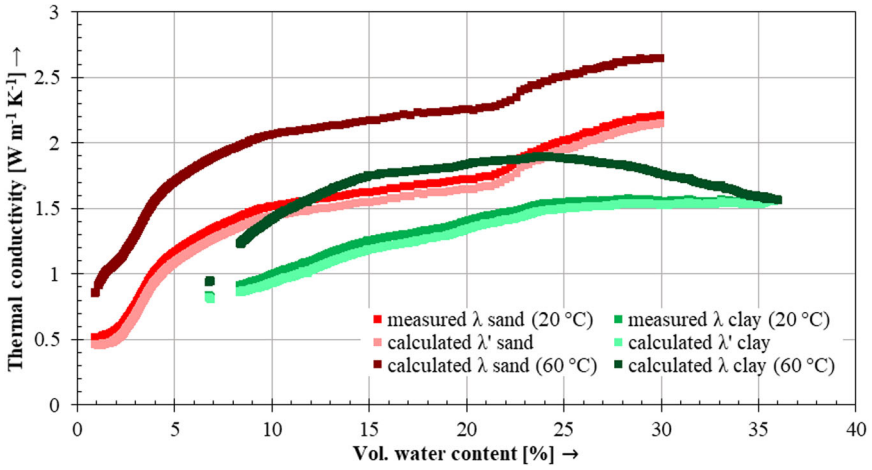

FIGURE 5 Measured apparent thermal conductivity λ at 20 ˚C and calculated thermal conductivity λ′ as well as λ at 60 ˚C of the sandy and clayey soil

2.3 | Theoretical background of the model

To compare the experimental data with a numerical model of coupled heat and mass transfer, a modified model was developed, based on the approach of Philip and de Vries (1957) and its adaption of Snijders et al. (1981). The equations summarized in this section were implemented in the simulation environment COMSOL Multiphysics to compare the model approach with the gathered experimental data of the tank experiment.

In this study the hydraulic potential h (m) is simplistically assumed by the sum of the matric potential and the gravitational potential Ψ_g (m):

$$h = \Psi_m + \Psi_g \tag{5}$$

According to the Darcy–Buckingham law (Buckingham, 1907), the water flow q_w (kg m^{-2} s^{-1}) depends on the unsaturated hydraulic conductivity k_u (m s^{-1}) and the hydraulic gradient:

$$q_w = -\rho_w(T)\, k_u(\theta, T)\, \nabla h \tag{6}$$

where ρ_w (kg m^{-3}) is the density of water and T (K) is the absolute temperature.

The complex microscopic interaction between solid grains with the liquid and gaseous phases and the two enduring together within the soil pores can be considered macroscopically by four diffusion processes (Philip & de Vries, 1957):

2.3.1 | Isothermal water transport

The isothermal flow of water follows gradients of the hydraulic potential. The isothermal water diffusivity coefficient $D_{\theta w}$ (m^2 s^{-1}) is describes as follows:

$$D_{\theta w}(\theta, T) = k_u(\theta, T) \left(\frac{\partial \Psi_m}{\partial \theta} \right) \tag{7}$$

The gradient is calculated in the model from the derivation of the used retention function.

The hysteresis is described in the model using the approach of Scott et al. (1983). For this purpose, each draining WRC is assigned the effective saturation function of the main drainage $S_{eff,dra}(\Psi)$ and the original parameter θ'_s is adjusted so that the equation intersects the starting point of a drainage:

$$\theta_{dra}\left(S_{eff,dra}\right) = \left(S_{eff,dra}\right)\left(\theta'_s - \theta_r\right) + \theta_r \tag{8}$$

In the case of an irrigating WRC, the effective saturation function of the main irrigation $S_{eff,irr}$ is used. The parameter of the residual water content θ'_r is adjusted in such a way that Equation 2 intersects the starting point of an irrigation.

$$\theta_{irr}\left(\Psi_m\right) = \left(S_{eff,irr}\right)\left(\theta_s - \theta'_r\right) + \theta'_r \tag{9}$$

Compared with the original formulation of Philip and de Vries (1957), the UHCC depends not only on the water content but also on the considered temperature. The temperature dependency of k_u through the viscosity and density of water was corrected in accordance with ISO Standard 17892-11 (2019):

$$k_{u,T} = k_{u,10°C} \frac{0.02414 \times 10^{[247.8/(T-273.15+133)]}}{0.02414 \times 10^{(247.8/143)}} \tag{10}$$

where T is the temperature (K) and $k_{u,10°C}$ is the hydraulic conductivity at 10 ˚C.

2.3.2 | Isohumid water transport

As the surface tension of water decreases with temperature, the matric potential is also subject to a change, resulting in a flow of water in the opposite direction of the temperature gradient. The thermal mass transfer of water follows these thermal induced hydraulic gradients. The isohumid diffusion coefficient of water D_{Tw} ($m^2\ s^{-1}\ K^{-1}$) is defined as follows:

$$D_{Tw}\ (\theta, T) = k_u\ (\theta, T)\ \left(\frac{\partial \Psi_m}{\partial T}\right) \tag{11}$$

The change of the matric potential, compared with a deviating reference temperature (e.g., temperature at measurement), is calculated according to Philip and de Vries (1957):

$$\Psi_m\ (T)\ = \frac{\sigma_T\ (T)}{\sigma_{T_{ref}}}\ \Psi_{m,T_{ref}} \tag{12}$$

where $\sigma_{T_{ref}}$ ($N\ m^{-1}$) is the surface tension and $\Psi_{m,T_{ref}}$ (m) is the matric potential at a reference temperature (like temperature at measurement of WRC).

The surface tension of water as a function of the temperature is described as follows (Dörfler, 1994).

$$\sigma_T\ (T)\ =\ 0.0728\ [1 - 0.002\ (T - 291)] \tag{13}$$

2.3.3 | Isothermal vapor transport

The isothermal vapor diffusion coefficient $D_{\theta v}$ ($m^2\ s^{-1}$) is calculated according to Snijders et al. (1981) as follows:

$$D_{\theta v}\ (\theta, T) =\ F\ (\theta) \times D\ (p, T) \times \frac{p}{p - p_v} \times \frac{g}{\rho_w\ (T)} \times \left(\frac{M_w}{RT}\right)^2 \times\ p_v \times \left(\frac{\partial \Psi_m}{\partial \theta}\right) \tag{14}$$

where $F(\theta)$ is a dimensionless correction factor regarding for the reduction of pore space by solid grains and extended effective diffusion paths through the tortuosity of the pore space, D ($m^2\ s^{-1}$) is the diffusion coefficient of vapor in air ($m^2\ s^{-1}$), p is the pore air pressure ($N\ m^{-2}$), p_v ($N\ m^{-2}$) the partial pressure of vapor, M_w ($kg\ kmol^{-1}$) molar mass of water, and the ideal gas constant $R = 8.314\ kJ\ kmol^{-1}\ K^{-1}$ and the gravitational acceleration g ($m\ s^{-2}$) are constant.

In Philip and de Vries (1957), it is assumed that a constant pressure of the gas phase prevails in the entire porous medium. This means that water vapor transfer is only caused by diffusion in stagnant air. In addition, the assumption of a saturated pore air in the entire medium applies.

The partial pressure of water has the following relationship to the relative humidity:

$$p_v\ =\ RH \times p_{v,sat} \tag{15}$$

where RH is the relative humidity. The temperature-dependent saturation vapor pressure of water at atmospheric pressure over a free water surface can be calculated by the Magnus formula according to Sonntag (1990):

$$p_{v,sat}\ (T) =\ 611.2\ \exp\left[\frac{17.52\ (T - 273.15)}{243.12 + (T - 273.15)}\right] \tag{16}$$

The thermodynamic equilibrium among the relative humidity, temperature, and matric potential is described in accordance with the Kelvin equation as follows (Or & Wraith, 2002):

$$\Psi_m\ (RH, T)\ = \rho_w\ (T)\ \frac{RT}{M_w}\ \ln\ (RH) \tag{17}$$

The diffusion coefficient of water vapor in air is calculated according to de Vries and Kruger (1967):

$$D\ (p, T)\ = D_0\ \left(\frac{p_0}{p}\right)\ \left(\frac{T}{T_0}\right)^{1.88} \tag{18}$$

With p_0 of 101,325 $N\ m^{-2}$, T_0 of 273.16 K, and D_0 of $21.7 \times 10^{-6}\ m^2\ s^{-1}$.

$F(\theta)$ is calculated as follows (Snijders et al., 1981): the critical moisture content θ_{crit} describes the moisture content in which liquid continuity is lost and

$$F\ (\theta) \begin{cases} = \varphi, & \text{if } \theta < \theta_{crit} \\ = (\varphi - \theta)\left(1 + \frac{\theta}{\varphi - \theta_{crit}}\right), & \text{if } \theta \geq \theta_{crit} \end{cases} \tag{19}$$

where ϕ ($m^3\ m^{-3}$) is the porosity and θ_{crit} is the critical moisture content in which liquid continuity is lost. The critical moisture content was set to 13% for the sandy and 15% for the clayey soil.

2.3.4 | Isohumid vapor transport

The thermal vapor diffusion coefficient is calculated according to Snijders et al. (1981):

$$D_{Tv}\ (\theta, T) =\ F\ (\theta) \times G \times D\ (p, T) \times \frac{p}{p - p_v} \times \frac{1}{\rho_w\ (T)} \times \frac{M_w}{RT} \times \frac{p_v}{p_{v,sat}\ (T, \Psi_m)} \times \left(\frac{dp_{v,sat}}{dT}\right) \tag{20}$$

where the thermal intensification factor G accounts for the influence of this thermal dispersion. Based on Philip and de Vries (1957), the value for G was assumed to be 1.8.

2.3.5 | Mass transport

According to the model of Philip and de Vries (1957), the movement of liquid water and vapor is calculated separately. The moisture flux q_m follows gradients of temperature or water content:

$$q_m = q_w + q_v \tag{21}$$

$$q_m = -\rho_w \left[\left(D_{\theta w} + D_{\theta v} \right) \nabla\theta + \left(D_{Tv} + D_{Tw} \right) \nabla T + k_u(T) \vec{e_z} \right] \tag{22}$$

The diffusion coefficients along the hydraulic gradient D_θ (m^2 s^{-1}) and the thermal gradient D_T (m^2 s^{-1} K^{-1}), respectively, can be combined (Philip & de Vries, 1957):

$$D_\theta = D_{\theta w} + D_{\theta v} \tag{23}$$

$$D_T = D_{Tw} + D_{Tv} \tag{24}$$

The change in the water content is described by

$$\frac{\partial\theta}{\partial t} = \nabla \left(D_{Tw} \nabla T \right) + \nabla \left(D_{\theta w} \nabla\theta \right) + \frac{\partial k_u}{\partial z} - E \tag{25}$$

where E (m^3 m^{-3} s^{-1}) is the rate of vaporization from water to vapor.

However, the water-based formulation in Philip and de Vries (1957) contains the firm restriction that hysteresis is not taken into account. For an implementation in numerical simulations, it is recommended not to use the saturation, but rather the hydraulic potential as a state variable, because its gradient is never zero and therefore is more robust in zones of high water content. In this case, Equation 25 changes to

$$\frac{\partial h}{\partial t} = \nabla \left(D_h^* \nabla h \right) \tag{26}$$

whereas the diffusion coefficients can be reformulated by using the chain rule:

$$D_\theta \nabla\theta = D_\theta \frac{\partial\theta}{\partial h} \nabla h = D_h^* \nabla h \tag{27}$$

2.3.6 | Heat transfer equations

As described in Snijders et al. (1981), the heat flux density $\vec{q}_{heat}$ (W m^{-2}) in porous media is described as the sum of the conductive heat transfer and the internal and latent energy contained in the mobile phases:

$$\vec{q}_{heat} = -\lambda' \nabla T + c_{p,w} \Delta T \vec{q}_w + \left[c_{p,v} \Delta T + L(T) \right] \vec{q}_v \tag{28}$$

where $c_{p,w}$ (J kg^{-1} K^{-1}) is the specific heat capacity of water, $c_{p,v}$ (J kg^{-1} K^{-1}) of vapor, and $\vec{q}_v$ the vapor flux (kg m^{-2} s^{-1}).

Due to the significant influence of the latent heat transfer, the temperature dependence of the latent heat of evaporation was additionally taken into account, in contrast with the original version according to Philip and de Vries (1957).

The specific enthalpy of vaporization of water as a function of temperature $L(T)$ (J kg^{-1}) is given by Anders and Radhakrishna (1988), based on data of Fowle (1921).

$$L(T) = 2.496 \times 10^6 - 2.37 \times 10^3 (T - 273.15) \tag{29}$$

The change of the temperature is described as follows:

$$c_p \frac{\partial T}{\partial t} = \nabla \left(\lambda' \nabla T \right) - L(T) \nabla \left(D_{\theta v} \nabla\theta \right) \tag{30}$$

where λ' (W m^{-1} K^{-1}) is the apparent thermal conductivity. The (conductive) thermal conductivity λ are in the following relationship to the apparent thermal conductivity (Philip & de Vries, 1957):

$$\lambda' = \lambda - L(T) \rho_w D_{Tv} \tag{31}$$

2.4 | Numerical implementation and simulation setup

All equations described before were implemented in the simulation environment COMSOL Multiphysics, using the mathematics module, together with the module for partial differential equations. It was found that the "MUMPS" solver delivered the fastest and—with regard to the stability—best result. Considerable effort was also put into the construction of the underlying mesh: a symmetrical mesh, consisting of a rectangle whose boundaries aligned with the nearly cylindrical isotherms lines provided the best results. Furthermore, a very fine meshing is necessary due to the large changes in hydraulic potentials at the boundary of the dry-out region. To compensate the fine meshing with respect to the calculation time, a linear Lagrange shape function was chosen for the geometric approximation of the variables. This has been found to deliver better results than a sparser mesh with a shape function of a

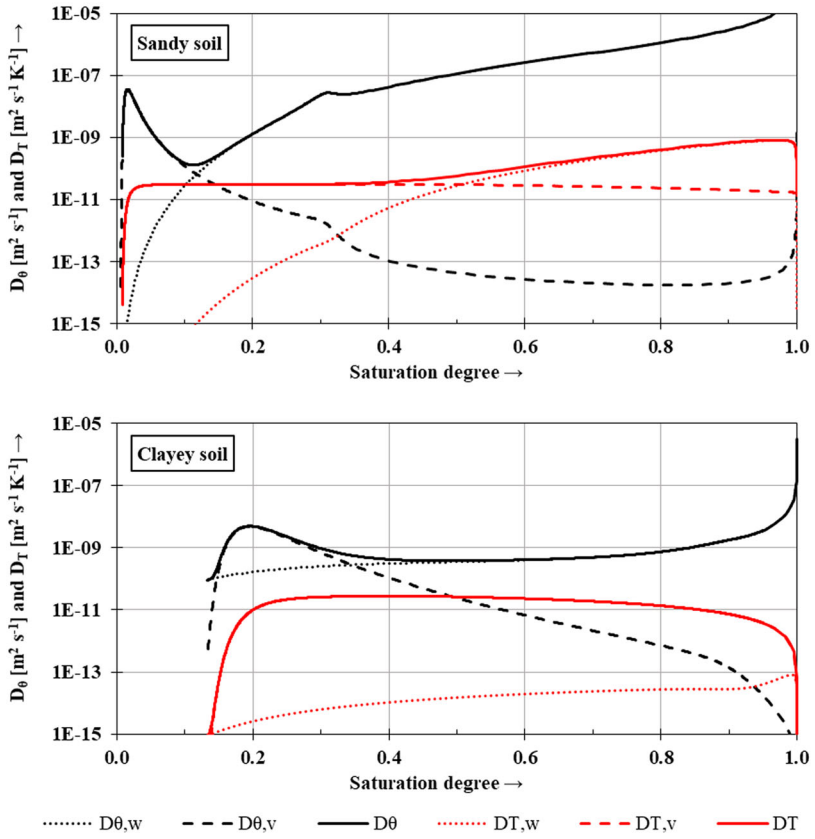

FIGURE 6 Diffusion parameters of the sandy and clayey soil, calculated from the experimental input data (case of main drainage at 20 °C). $D_{\theta,w}$, isothermal water diffusivity coefficient; $D_{\theta,v}$, isothermal vapor diffusivity coefficient; D_{θ}, isothermal moisture diffusivity coefficient; $D_{T,w}$, isohumid water diffusivity coefficient; $D_{T,v}$, isohumid vapor diffusivity coefficient; D_{T}, isohumid diffusivity coefficient

higher order. The time variant simulation starts directly after inserting the bedding material into the experimental setup. The measured water content and matric potential (for taking into account the hysteresis via Equations 8 and 9) at this point were used as the initial conditions of the simulation. The temperatures on the central heating pipe and the outer steel tank measured during the experiment were set as boundary conditions. The measured apparent thermal conductivity is described in the model using a linear interpolation of the measured values.

3 | RESULTS AND DISCUSSION

3.1 | Calculated diffusion coefficients of the investigated soils

The soil properties presented in Section 2 were used to calculate the four diffusion coefficients using Equations 7, 11, 14, and 20. These diffusion coefficients govern the mass transfer and, therefore, the heat transfer within the unsaturated soil. For the sandy soil, the results as a function of saturation are presented in the upper diagram and for the clayey soil in the lower diagram of Figure 6. In analyzing the curves of the sandy soil, the causes behind the drying-out can be comprehended: it can be stated that the diffusion coefficient along moisture gradients D_{θ} reaches a minimum at about 13% saturation, where the transfer of liquid diminishes sharply with the interruption of liquid water bridges inside the soil. As a consequence of D_{θ} reaching its minimum, the gradient of the saturation has to increase, leading to the formation of a dry-out zone.

By comparing the curves of both soils, the difference is obvious: as there is no sudden decrease from the hydraulic conductivity in fine-grained soils with decreasing water content, the diffusion coefficient D_{θ} of the clayey soil does not have such a distinctive minimum as in coarse-grained soils.

3.2 | Comparison of tank experiment and simulations

Figure 7 shows excerpts from the measured temperatures and matric potentials as well as the related simulation results of the tank experiment. The measured values of the investigated soils, the detailed position of sensors, as well as the complete measurement series of the tank experiments are available online as referred to in the data availability section. Since the measurement range of the tensiometers is limited in the dry range up to around −8.5 m, unfortunately the second test series of the sandy soil was slightly too dry, and no hydraulic data could be gathered. Thus, only temperature data were

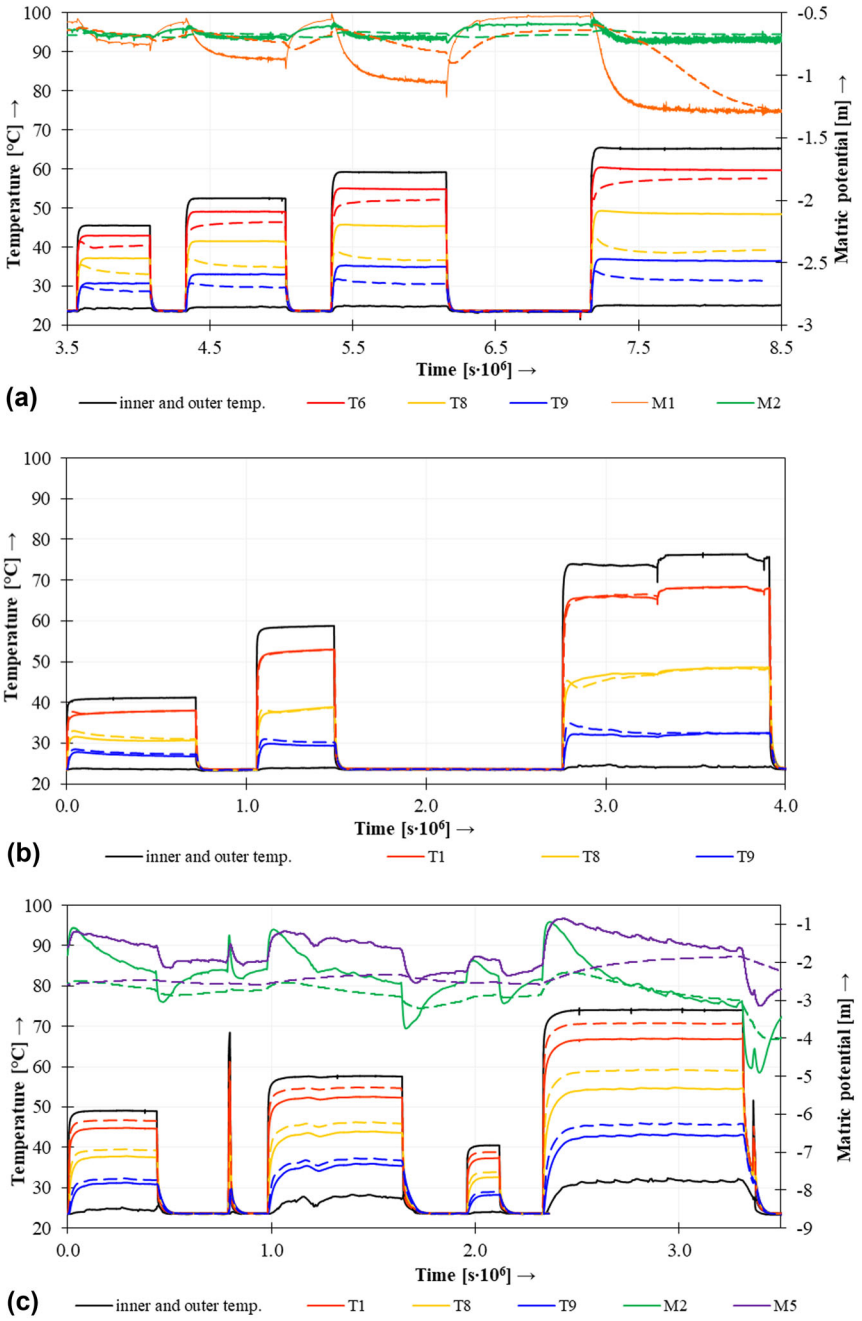

FIGURE 7 Measured (solid lines) and simulated (dashed lines) time series. (a) Sandy soil saturation = 32%; (b) sandy soil saturation = 14%; (c) clayey soil saturation = 82%

available for the test series of the dry sandy soil. The repetition of single temperature measurement steps (phases of constant temperature differences between the inner and outer pipe) in all measurement series showed a high degree of reproducibility. The differences between simulation and experiment will be exemplified by means of selected temperature pulses, whereas the presented interrelations could be found in all series of measurements carried out in one test series. It is apparent from Figure 7 that the measured temperatures (solid lines) reached a constant level in a short time after the beginning of each heating cycle. The matric potential, on the other hand, shows a significantly delayed behavior, related due to the slower progressing changes in the water content.

The measured temperatures in Figure 7b show the effect of a slowly expanding area of drying-out around the heat source. Moreover, the drying-out by a temperature gradient is many times faster than a rewetting caused only by a moisture gradient—for example, in between the heat pulses. With the simulation of the sand of 14% saturation, it was demonstrated that the drying-out of the soil persists, even when the heating was switched off for several days. The simulated dynamics of the matric potential of the moist sand are described too slowly. The variations in the water content due to temperature

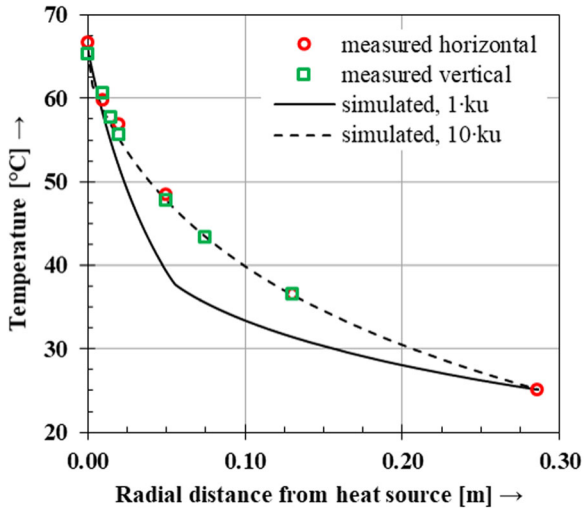

FIGURE 8 Measured and simulated temperature at radial distance to the heat source in test series of sand with initial saturation of 32% ($t = 8.4 \times 10^6$ s). Horizontal measurements: T14, T6, T7, T8, T9, T15; Vertical measurements: T5, T10 T1, T2, T3, T11, T4. The k_u is the unsaturated hydraulic conductivity

gradients is underestimated. In the comparatively impermeable material of the clayey soil, the sudden changes in temperature lead to a brief pneumatic potential, which influences the tensiometer measurements. Apart from the fact that this was not taken into account in the simulation, these potentials are well described.

Despite the care taken in the experimental determination of the input data and their implementation in the physical model, the calculations with the model sometimes show deviations from the measured values. Deviations in the temporal development of the temperatures after applying a temperature gradient indicate deviations in the description of a developing drying process. Since even a minor drying area near the heat source has a large influence on the heat dissipation, the spatial resolution of the measurement equipment used in the tank experiment is limited by its size. Figure 8 shows the spatial distribution of the temperatures during the end of the last temperature pulse shown in Figure 7a at 8.4×10^6 s.

The simulated result showed a large dry-out zone of around 5 cm (indicated by the change of slope of the temperature curve). This thermally insulating zone resulted in a reduced heat flux and in lower temperatures in the whole bedding.

There are several possibilities that might have led to these discrepancies. From the experimental aspect, mainly uncertainties in the determination of hydraulic input parameters seem to be plausible. At the initial saturation of the investigated soils, $D_{\theta w}$ and D_{Tv} dominated the transport of water and thus the drying-out processes. In the saturation state of all samples examined, a reduction in hydraulic conductivity leads to a decrease in D_θ by domination of $D_{\theta w}$. This increasingly restricts the transport of liquid water to the heat source, whereas the transport of vapor in opposite direction remains unaffected. $D_{\theta w}$ is subject to errors from the hydraulic conductivity and the slope of the retention function. Exemplarily the hydraulic conductivity was increased by 10 times for the simulation shown in Figure 8, and a much better fit to the experimental was achieved. The diffusion of water vapor along temperature gradients is described by the diffusion coefficient D_{Tv}. According to Snijders et al. (1981) D_{Tv} was calculated from the measured value of the pore space fraction and an assumption about the critical water content. Errors in both quantities influence the value of D_{Tv}, albeit to a small extent. As part of a sensitivity analysis, the causes of the deviations can be narrowed down on the basis of experimental data presented here, and this model can be optimized, or other models can be validated. Hence, it has to be considered that data of evaporation tests cannot directly ensure a correct calculation of the heat and mass transfer especially to higher matric potentials. For simulations, continuous functions are usually used to describe hydraulic properties. Deviations in a function fitted to measured values also contribute to deviations in such a simulation. These uncertainties can affect the calculation of the drying-out process and thus also the thermal conditions around cables.

4 | CONCLUSION

The application of a coupled heat and mass transfer model requires an experimental validation, as well as adequate input data. This study presents a possible approach by using high resolution experimental data, collected with a specially built experimental setup. Furthermore, all input parameters were experimentally determined. These input data were used in a model approach to simulate the different test series of the tank experiment. Some differences in the temporal changes of temperatures and matric potentials were identified.

For the validation of coupled heat and mass transfer models, temperature and hydraulic data at high temporal and spatial resolution are needed. The test series conducted with the two soils emphasized that, especially for the hydraulics, it is a problem to gain high-resolution data in the dry range. Although tensiometers are probably the best systems to investigate the hydraulic situation in such an environment, their limited measurement range is a restriction when studying forced drying effects such as in the case of heated power cables.

Nevertheless, the experimental data published with this study are useful to validate model approaches for the description of the drying effects around buried cables. By correctly describing the dynamics and the extent of the drying-out effects, these approaches might also be used for calculations under variable boundary conditions, such as those encountered in practical application. Considering these more detailed

bedding properties, an intelligent power flow management system could allow for a more efficient load capacity of cable routes at simultaneously higher safety against thermal damage.

ACKNOWLEDGMENTS

We thank E.ON Innovation Center Distribution and Bayernwerk AG for financial support. Parts of this work were also financially supported by the DFG in the framework of the Excellence Initiative, Darmstadt Graduate School of Excellence Energy Science and Engineering (GSC 1070). We acknowledge support by the Deutsche Forschungsgemeinschaft (DFG—German Research Foundation) and the Open Access Publishing Fund of Technical University of Darmstadt. The authors are further grateful for the constructive comments of two anonymous reviewers.

AUTHOR CONTRIBUTIONS

Christoph Verschaffel-Drefke: Conceptualization; Formal analysis; Investigation; Methodology; Validation; Visualization; Writing-original draft; Writing-review & editing. Constantin Balzer: Conceptualization; Software; Writing-review & editing. Markus Schedel: Data Curation; Formal analysis; Writing-review & editing. Volker Hinrichsen: Funding acquisition; Supervision; Writing-review & editing. Ingo Sass: Funding acquisition; Supervision; Writing-review & editing.

CONFLICT OF INTEREST

The authors declare no conflict of interest.

DATA AVAILABILITY STATEMENT

The data from the conducted experiments and the investigated soils are available online: https://doi.org/10.48328/tudatalib-644.

ORCID

Christoph Verschaffel-Drefke https://orcid.org/0000-0002-8538-7667
Markus Schedel https://orcid.org/0000-0001-6596-831X

REFERENCES

Anders, G. J., & Radhakrishna, H. S. (1988). Power cable thermal analysis with consideration of heat and moisture transfer in the soil. *IEEE Transactions on Power Delivery*, *3*(4), 1280–1288. https://doi.org/10.1109/61.193921

Brakelmann, H. (1984). *Physical principles and calculation methods of moisture and heat transfer in cable trenches* (Etz-report 19). VDE-Verlag.

Buckingham, W. (1907). *Studies on the movement of soil moisture* (Bulletin 38). USDA.

Childs, E. C. (1969). *An introduction to the physical basis of soil water phenomena*. Wiley-Interscience.

de Vries, D. A., & Kruger, A. J. (1967). Phénomènes de transport avec changement de phase dans les milieux poreux ou colloidaux. *Centre national de la recherche scienfique*.

Dörfler, H. D. (1994). *Grenzflächen-und Kolloidchemie*. VCH Verlag.

Drefke, C., Schedel, M., Stegner, J., Balzer, C., Hinrichsen, V., & Sass, I. (2017). Measurement method of thermal properties of cementitious bedding materials and unsaturated soils: Hydraulic influence on thermal parameters. *Geotechnical Testing Journal*, *40*(1), 160–170. https://doi.org/10.1520/GTJ20160027

Drefke, C., Stegner, J., Dietrich, J., & Sass, I. (2015). Influence of the hydraulic properties of unconsolidated rocks and backfill materials on the change of the thermophysical characteristics by heat transfer. In *Proceedings World Geothermal Congress 2015*. International Geothermal Association.

Durner, W. (1994). Hydraulic conductivity estimation for soils with heterogeneous pore structure. *Water Resources Research*, *30*(2), 211–223. https://doi.org/10.1029/93WR02676

Freitas, D. S., Prata, A. T., & de Lima, A. J. (1996). Thermal performance of underground power cables with constant and cyclic currents in presence of moisture migration in the surrounding soil. *IEEE Transactions on Power Delivery*, *11*(3), 1159–1170. https://doi.org/10.1109/61.517467

Fowle, F. E. (Ed.). (1921). *Smithsonian physical tables* (7th ed.). Smithsonian Institution.

Groeneveld, G. J., Snijders, A. L., Koopmans, G., & Vermeer, J. (1984). Improved method to calculate the critical conditions for drying out sandy soils around power cables. *IEEE Proceedings*, *131*(2), 42–53. https://doi.org/10.1049/ip-c.1984.0007

Hillel, D. (1980). *Fundamentals of soil physics*. Academic Press.

Hruška, M., Clauser, C., & De Doncker, R. W. (2018). The effect of drying around power cables on the vadose zone temperature. *Vadose Zone Journal*, *17*(1), 1–15. https://doi.org/10.2136/vzj2018.05.0105

ISO Standard 17892-11. (2019). *Geotechnical investigation and testing—Laboratory testing of soil—Part 11: Permeability tests*. International Organization for Standardization.

Kroener, E., Campbell, G. S., & Bittelli, M. (2017). Estimation of thermal instabilities in soils around underground electrical power cables. *Vadose Zone Journal*, *16*(9), 1–13. https://doi.org/10.2136/vzj2017.04.0082

Kroener, E., Vallati, A., & Bittelli, M. (2014). Numerical simulation of coupled heat, liquid water and water vapor in soils for heat dissipation of underground electrical power cables. *Applied Thermal Engineering*, *70*(1), 510–523. https://doi.org/10.1016/j.applthermaleng.2014.05.033

Mualem, Y. (1976). A new model for predicting the hydraulic conductivity of unsaturated porous media. *Water Resources Research*, *12*(3), 513–522. https://doi.org/10.1029/WR012i003p00513

Or, D., & Wraith, J. M. (2002). Soil water content and water potential relationships. In A. Warrick (Ed.), *Soil physics companion* (pp. 49–84). CRC Press.

Pertassek, T., Peters, A., & Durner, W. (2011). *HYPROP data evaluation software: User's manual, V.1.0*. United Mobile Services.

Peters, A., Iden, S. C., & Durner, W. (2015). Revisiting the simplified evaporation method: Identification of hydraulic functions considering vapor, film and corner flow. *Journal of Hydrology*, *527*, 531–542. https://doi.org/10.1016/j.jhydrol.2015.05.020

Philip, J. R., & de Vries, D. A. (1957). Moisture movement in porous materials under temperature gradients. *Transaction American*

Geophysical Union, *38*(3), 222–232. https://doi.org/10.1029/TR038i002p00222

Priesack, E., & Durner, W. (2006). Closed-form expression for the multi-modal unsaturated conductivity function. *Vadose Zone Journal*, *5*(1), 121–124. https://doi.org/10.2136/vzj2005.0066

Radhakrishna, H. S., Lau, K. C., & Crawford, A. M. (1984). Coupled heat and moisture flow through soils. *Journal of Geotechnical. Engineering*, *110*(12), 1766–1784. https://doi.org/10.1061/(ASCE)0733-9410(1984)110:12(1766)

Saito, H., Šimůnek, J. &., & Mohanty, B. P. (2006). Numerical analysis of coupled water, vapor, and heat transport in the vadose zone. *Vadose Zone Journal*, *5*(2), 784–800. https://doi.org/10.2136/vzj2006.0007

Schindler, U., Durner, W., von Unold, G., & Müller, L. (2010). Evaporation method for measuring unsaturated hydraulic properties of soils: Extending the measurement range. *Soil Science of Society of America Journal*, *74*(4), 1071–1083. https://doi.org/10.2136/sssaj2008.0358

Scott, P. S., Farquhar, G. J., & Kouwen, N. (1983). Hysteretic effects on net infiltration. In *Proceedings of a of National Conference on Advances in Infiltration* (Publ. 11-83, pp. 163–170). American Society of Agricultural and Biological Engineers.

Snijders, A. L., Groenveld, G. J., Vermeer, J., & van de Wiel, G. M. L. M. (1981). Moisture migration and drying-out in sand around heat dissipating cables and ducts - A theoretical and experimental study. KEMA.

Sonntag, D. (1990). Important new values of the physical constants of 1986, vapour pressure formulations based on the ITC-90 and psychrometer formulae. *Zeitschrift fuer Meteorologie*, *40*(5), 340–344.

How to cite this article: Verschaffel-Drefke, C., Balzer, C., Schedel, M., Hinrichsen, V., & Sass, I. (2022). Experiment for validation of numerical models of coupled heat and mass transfer around energy cables. *Vadose Zone J. 21*, e20173. https://doi.org/10.1002/vzj2.20173